Scientific Research Publishing

Open Journal of Applied Sciences, 2026, 16(5), 1793-1811
https://www.scirp.org/journal/ojapps
ISSN Online: 2165-3925
ISSN Print: 2165-3917

Experimental Assessment of Solar Irradiance in Kankan and Validation of a Photovoltaic Resource Prediction Model

Namory Diaby[1,2], Mohamed Ansoumane Camara[1,2*], Souleymane Soumah[1,2], Ansoumane Sakouvogui[3]

[1]Laboratory for Teaching and Research in Energetics and Automation (LENA), University Gamal Abdel Nasser de Conakry (UGANC), Conakry, Guinea
[2]Department of Electrical Engineering of the Polytechnic Institute, UGANC, Conakry, Guinea
[3]Higher Institute of Technology of Mamou, Mamou, Guinea
Email: namorydiabi@gmail.com, *mohamedansoumane@gmail.com, soulems38@gmail.com, ansoumane2015@gmail.com

How to cite this paper: Diaby, N., Camara, M.A., Soumah, S. and Sakouvogui, A. (2026) Experimental Assessment of Solar Irradiance in Kankan and Validation of a Photovoltaic Resource Prediction Model. *Open Journal of Applied Sciences*, **16**, 1793-1811.
https://doi.org/10.4236/ojapps.2026.165099

Received: April 4, 2026
Accepted: May 22, 2026
Published: May 25, 2026

Abstract

Assessing solar resources is essential for estimating a region's energy potential in terms of photovoltaic energy production. In Guinea, although average sunshine levels are high (around 4.8 kWh/m^2/day), exploitation of this resource remains limited, particularly in rural areas. Upper Guinea, with its 2700 hours of sunshine per year and dry climate, offers ideal conditions for solar development. However, the lack of reliable weather stations is a major obstacle. To overcome this constraint, we have set ourselves the goal of conducting an experimental study to measure and evaluate solar irradiance in Kankan, using a system of equipment equipped with an autonomous pyranometer. To capture variations in solar irradiance, a sampling interval of 5 minutes was chosen. Measurements were taken over a period of more than one year, but in this study we focused on data from one week of measurements (April 12 to 18, 2025). These measurements revealed high solar potential, with peaks reaching 1000 to 1100 W/m^2 in some places. The curves obtained reveal both the regularity of the solar cycle and meteorological variability. The next step in our work will be a comparative study between the data measured on site and the results obtained using a code developed in previous work, specifically, a clear-sky irradiance model, for the first day of measurement (April 12, 2025). We will then conclude with a correlation study between these two sets of data.

Keywords

Solar Resource, Irradiance, Pyranometer, Photovoltaics, Correlation

1. Introduction

Interest in developing solar energy in West Africa is growing rapidly, driven by high solar radiation potential and the need to improve access to electricity [1] [2]. The Upper Guinea region, and in particular the prefecture of Kankan, has annual levels of solar radiation that are highly favorable for photovoltaic applications, but the optimal exploitation of this resource depends on the accuracy of local irradiance estimates [3].

The performance and reliability of photovoltaic feasibility studies rely heavily on the quality of the irradiance data used. Numerous studies show that satellite and reanalysis data, although essential for large-scale mapping, present uncertainties related to cloud cover, Sahelian aerosols, and local microclimatic variability [4]-[6]. Therefore, ground measurements taken with pyranometers compliant with ISO 9060 remain essential for accurately characterizing solar resources, validating satellite products, and improving the robustness of prediction models [7].

Furthermore, the integration of photovoltaic systems with battery storage (PV-BESS) requires accurate, high-resolution temporal knowledge of irradiance in order to optimize load management strategies, energy planning, and battery longevity [8] [9]. Recent work highlights that rapid variations in solar radiation directly influence actual energy performance, the optimal sizing of stand-alone PV systems, and the overall performance ratio [10].

In this context, this study proposes an experimental study to measure and evaluate solar irradiance in Kankan, followed by a detailed statistical analysis of daily profiles. It also examines the results of correlation parameters obtained when comparing experimental data with data provided by the solar resource assessment code for the site under study. This approach will make it possible to better size autonomous photovoltaic systems and, consequently, optimize their performance. Finally, the results obtained will offer the possibility of adjusting or correcting satellite estimates of solar irradiance data for the region under consideration.

The rest of the article is structured as follows: Section 2 presents the study site, the measurement equipment used, and the methodology applied. Section 3 analyzes the results using daily profiles, statistical tools, and linear regression. Finally, Section 4 concludes the study by highlighting the main findings, recommendations, and prospects for future related work.

2. Materials and Methods

2.1. Materials

2.1.1. Site Description

The experiment and measurements were conducted at Julius Nyerere University in Kankan. This Guinean public university was founded in 1964 under the name Secondary Teacher Training College and in 1989 it was renamed Julius Nyerere University of Kankan (Decree No. 175/PRG/SGG/89 of September 27, 1989).

The population of the city of Kankan (March 2022) is estimated at 194,671 inhabitants (99,168 men and 95,503 women) [11]. Its area is approximately 11,564

km² [12]. The capital, the city of Kankan, is located at 10.3835˚N, 9.3069˚W [13], with an average altitude of approximately 380 - 400 m [14].

Climatically, Kankan is in a Sudano-Guinean savanna zone, with two distinct seasons: a dry season from November to April and a rainy season from May to October [15]. Average temperatures range from 25˚C to 35˚C, with peaks of up to 40˚C in the dry season [16]. Annual rainfall is approximately 1534 mm, spread over an average of 122 rainy days [16].

The terrain of the prefecture is characterized by a relatively flat plateau, cut by a few shallow river valleys; some parts reach 500 m, but most are between 400 and 420 m, while to the south there are heights of up to 650-700 m, and even ± 800 m in some places [17]. **Figure 1** presents the map of the study area.

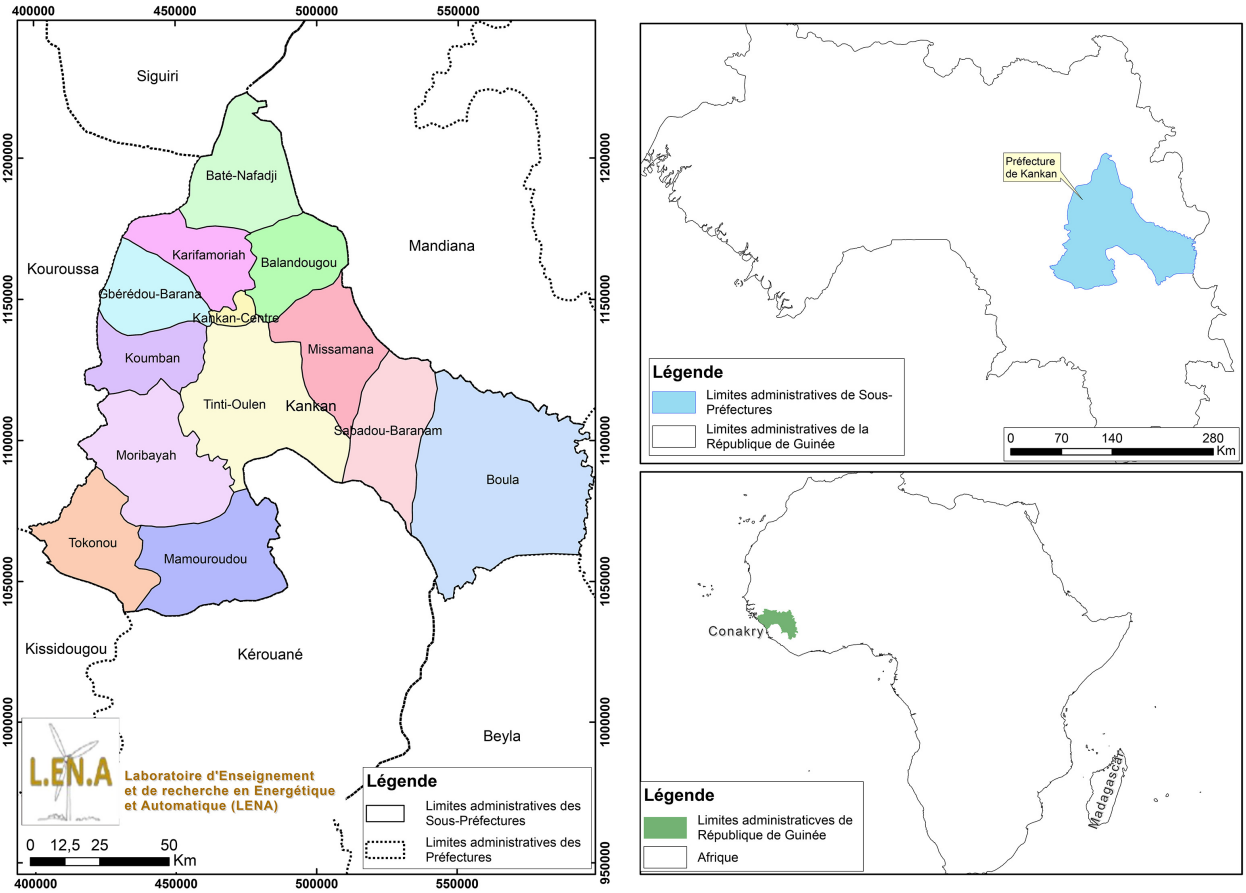

Figure 1. Map of Kankan prefecture with its thirteen (13) sub-prefectures (Source: Original created by us using QGIS software).

The dominant vegetation is that of shrubby savanna/wooded savanna, punctuated by forest galleries along the watercourses [18]. Species such as acacia, melina, and other fruit trees are found in inhabited areas [16].

Administratively, it is bordered to the north by the prefectures of Siguiri and Mandiana, to the south by Kérouané and Kissidougou, to the east by the prefecture of Mandiana and the Republic of Ivory Coast, and to the west by the prefecture of Kouroussa [19].

The population of the Kankan region is divided between the urban commune and the following twelve rural sub-prefectures: Boula, Sabadou-Baranama, Missamana, Balandou, Batè-Nafadji, Gbérédou-Baranama, Koumban, Moribaya, Tintioulen, Tokounou, Karifamoriah, and Mamouroudou [20].

The city of Kankan experiences frequent power cuts due to insufficient electricity production. This situation disrupts the daily lives of residents and has a considerable impact on the city's economic activities.

2.1.2. Description of the Equipment Installed to Measure Solar Irradiance

The measurements were taken using a pyranometer (**Figure 2(b)**), a highly accurate measuring device designed to quantify the total solar radiation received on a surface. The complete solar irradiance measurement equipment installed on the roof of a building at the University of Kankan is shown in **Figure 2(a)**. This measuring device is combined with an instrument that requires continuous monitoring, called a "data logger". This equipment is designed to automatically collect and record the measured solar irradiance data.

A photovoltaic module was used as an autonomous power source for the data logger. This arrangement ensures that the equipment and system operate normally and without interruption, guaranteeing reliable data collection on site.

(a) (b)

Figure 2. View of the solar irradiance measurement equipment system installed on the roof of a building at the University of Kankan. (a) Solar irradiance measurement equipment installed on site; (b) Pyranometer.

The schematic diagram of solar irradiance capture at the site, showing the system equipment, is presented in the figure below (**Figure 3**).

The system studied consists of a solar panel connected to a charge controller, which is itself connected to a battery, ensuring a constant and uninterrupted power supply to the data logger and the rest of the system. For the measurement and collection of solar irradiance data, a sampling interval of five minutes was chosen when configuring the device. This choice makes it possible to accurately detect small fluctuations and reliably observe changes in the data measured on site.

The evolution of the data measured during the first seven (7) days of collection is illustrated by the curves in the figures below.

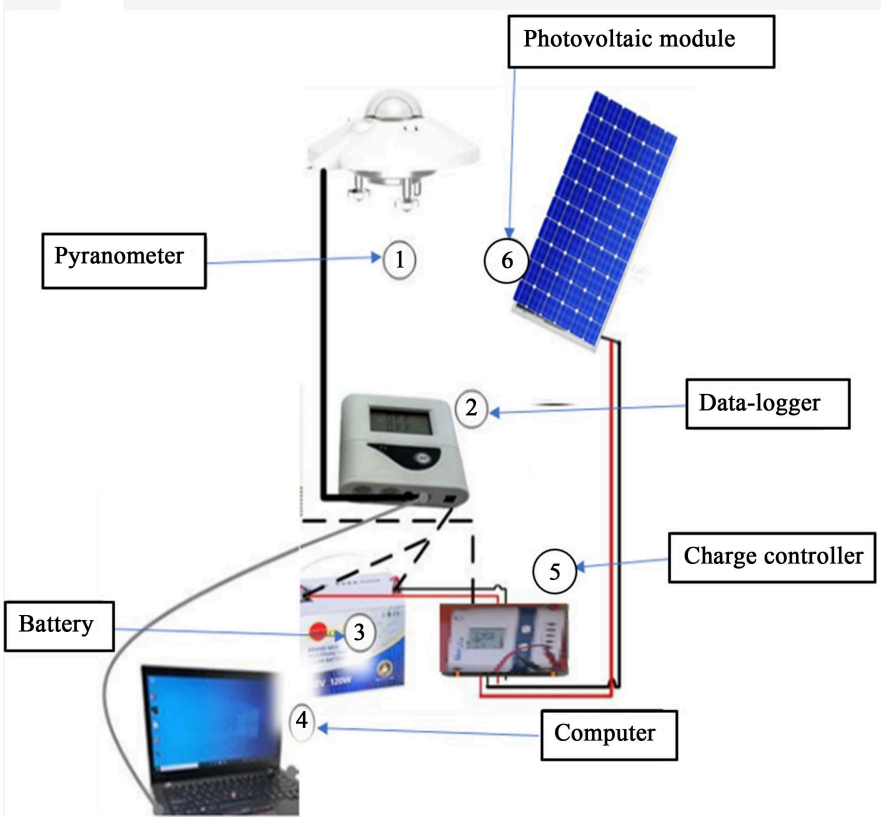

Figure 3. System consisting of combined devices for collecting experimental data.

2.1.3. Data Collected on Site: Solar Irradiance for the Seven (07) Days of Measurements

The seven curves (Figures 4-10) illustrate the evolution of solar irradiance (in W/m^2) measured on site from April 12 to 18, 2025, during the various days of measurement, between approximately 7:00 a.m. and 6:00 p.m.

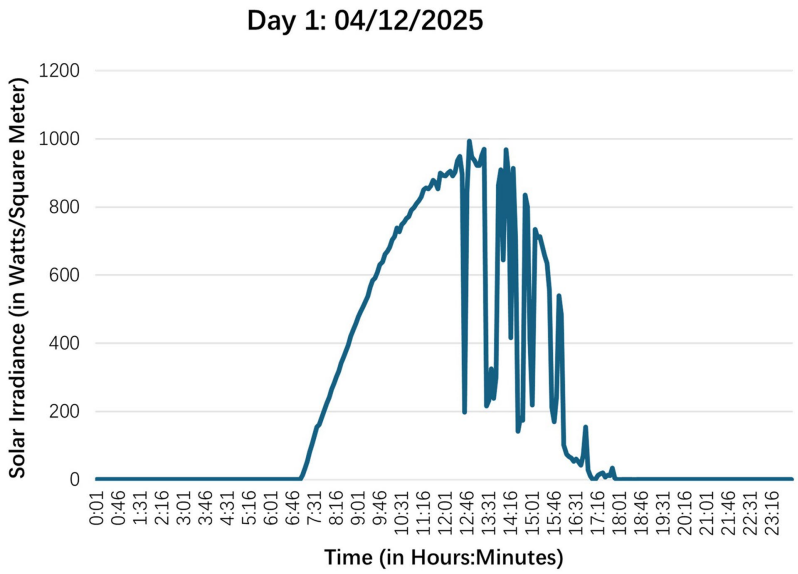

Figure 4. Daylighting 1.

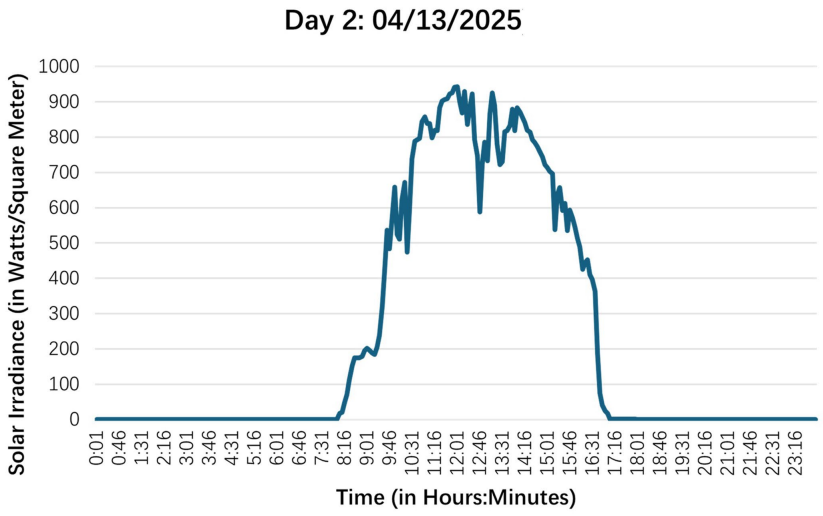

Figure 5. Daylighting 2.

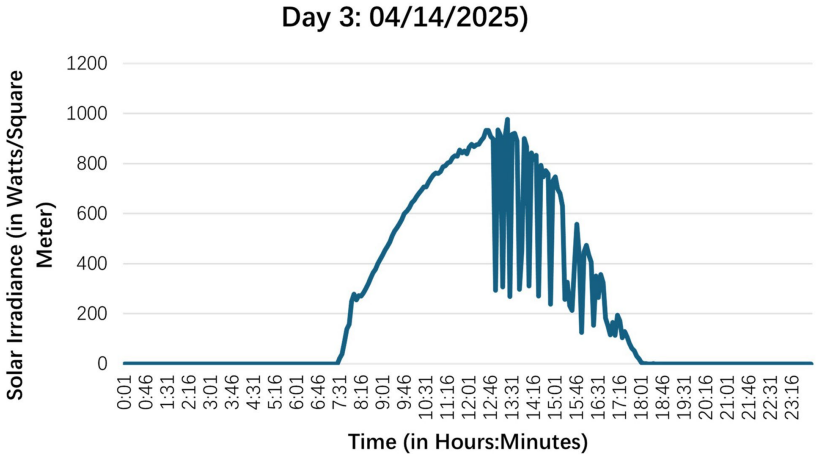

Figure 6. Daylighting 3.

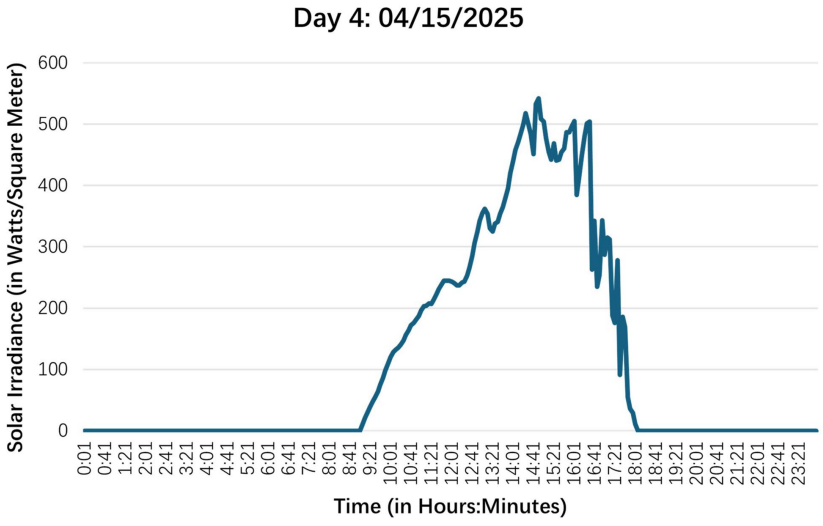

Figure 7. Daylighting 4.

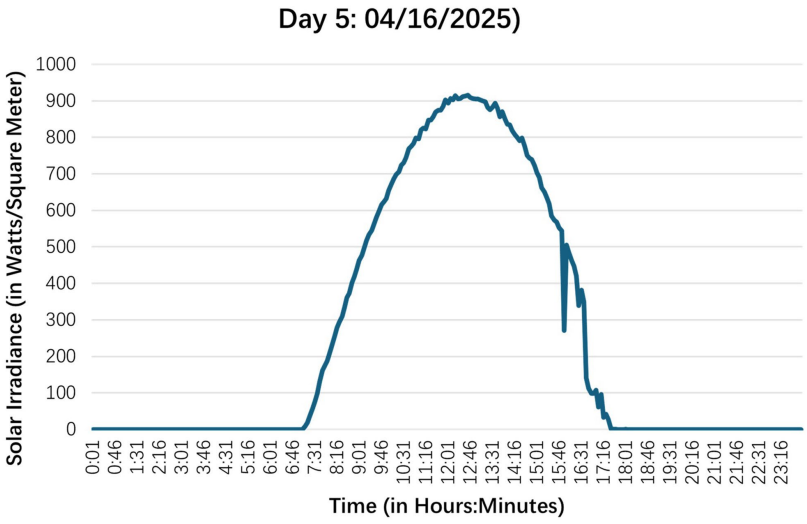

Figure 8. Daylighting 5.

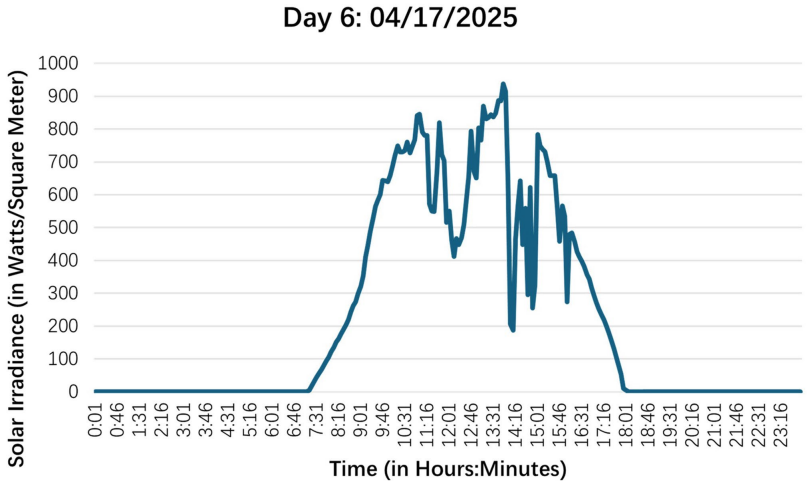

Figure 9. Daylighting 6.

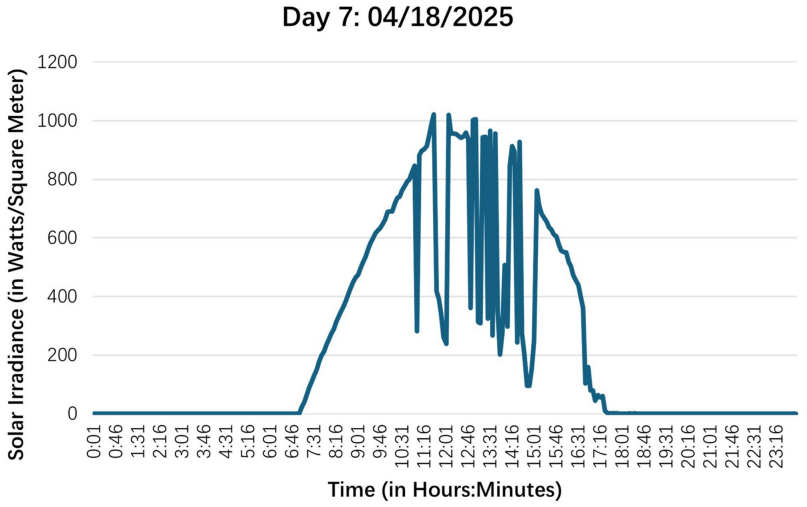

Figure 10. Daylighting 7.

Overall, all curves are quasi-parabolic in shape, characteristic of the daily cycle of solar radiation:

- a gradual increase in the morning,
- a maximum around noon (when the Sun is at its zenith),
- then a symmetrical decrease in the afternoon.

Regarding variability between days:

The curves for days 1, 3, 5, and 7 are relatively regular, with a clear peak and a symmetrical shape, characteristic of generally sunny days.

Days 2 and 6 show several sharp drops in illuminance before and after noon, which can be explained by intermittent cloud cover.

Day 4 shows significantly lower irradiance, peaking at around 550 W/m^2: a very overcast or foggy day.

Regarding the observed irradiance levels:

The maximum values reach approximately 1000 to 1100 W/m^2, corresponding to strong sunlight, typical of a clear sky in the middle of the day.

The minimum values close to zero before 7 a.m. and after 6 p.m. clearly reflect the absence of nocturnal irradiance.

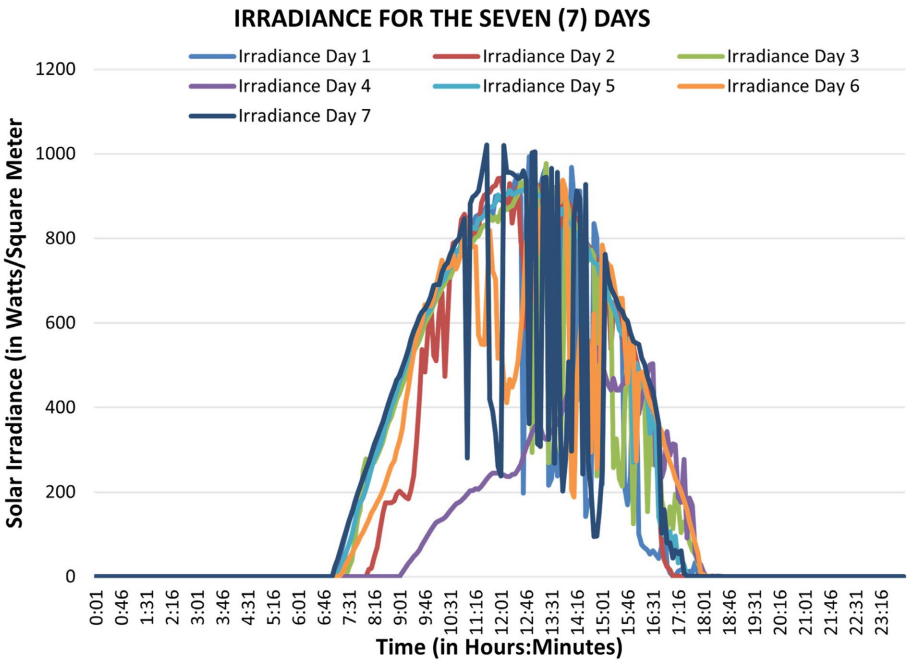

Figure 11. Common representation and comparison of solar irradiance for the first seven days of measurements.

Figure 11 shows the curves representing the daily variation in solar irradiance during the first seven days of measurement. All seven curves show a typical daily solar irradiance profile, rising in the morning, peaking at midday between 11:30 a.m. and 1:00 p.m., and then decreasing in the afternoon.

The differences in amplitude between days reveal variable cloud cover conditions, with maximum sunshine on days 1, 3, 5, and 7, and reduced illumination

on days 2, 4, and 6.

The hourly trends observed show the following results:

- A gradual increase in the morning
- Irradiance begins around 6:30-7:00 a.m., reflecting sunrise.
- The maximum is observed between 11:30 a.m. and 1:00 p.m., depending on the day.
- The decrease is gradual until 6:00 p.m., at which time the illumination drops to zero.

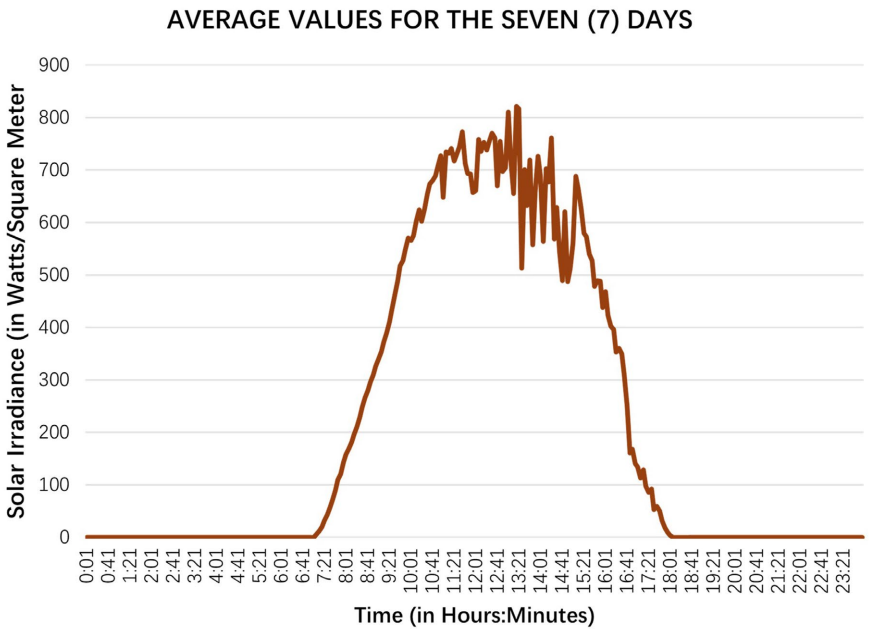

Figure 12. Average illuminance values for the first seven days of measurement.

The graph in **Figure 12**, which shows the average solar irradiance curve over a seven-day period, highlights a typical day characterized by a steady increase in radiation from 6:30 a.m., followed by a plateau of high intensity between 10:00 a.m. and 2:00 p.m., reaching approximately 800 W/m^2, then a gradual decrease until 6:00 p.m.

The fluctuations observed around the maximum reflect atmospheric variability between the days considered, but the overall high level of average irradiance confirms significant solar potential and favorable conditions for photovoltaic energy production during this period.

2.2. Methods

2.2.1. Evaluation of Illuminance Using a Code and Comparison with Data Collected on Site

The measured solar illuminance values are compared with those obtained using the solar resource evaluation code, which corresponds to a clear-sky irradiance model based on the Linke turbidity factor, as developed and validated in the previous work cited in [21], enabling a physically based estimate of solar radiation

based on local atmospheric conditions.

In this model [22], expression (1) is used to evaluate the different solar irradiance values measured on site.

$$G_{i,\gamma} = S^*_{i,\gamma} + D^*_i \tag{1}$$

where:

- $G_{i,\gamma}$: is the global radiation on a flat surface with an inclination i and orientation γ relative to the south direction;
- $S^*_{i,\gamma}$: is the useful component of direct illumination;
- D^*_i : is the diffuse radiation received by the plane with inclination i.

The sum of direct radiation and diffuse radiation constitutes global radiation.

The useful component of direct illumination ($S^*_{i,\gamma}$)

$$S^*_{i,\gamma} = I^*_0 \left[\cos h \cdot \sin i \cdot \cos(a-\gamma) + \sin h \cdot \cos i \right] \tag{2}$$

with I^*_0, **the direct radiation at ground level:**

$$I^*_0 = \overline{I^*_0} \exp\left[-\frac{m_h T_L}{0.9 \cdot m_h + 9.4} \right] \tag{3}$$

where:

- h and a, are the horizontal celestial coordinates, respectively: the height and azimuth of the point to be located.
- $\overline{I^*_0}$: is the solar constant or extraterrestrial solar radiation with a value of 1366 W/m^2.

The atmospheric optical distance (m_h):

The atmospheric optical distance, also known as atmospheric mass (in m), takes into account the path traveled by photons as they pass through the Earth's atmosphere.

The atmospheric optical depth is equal to the ratio of the distance traveled in the atmosphere by a ray from the Sun to the vertical thickness of the atmosphere measured at sea level.

It is expressed using the height of the Sun (h), according to the following relationship:

$$m_h = \frac{1 - 0.1 \cdot z}{\sin h + 0.15 \cdot (h + 3.885)^{-1.253}} \tag{4}$$

where:

- z is the altitude of the location,
- at sea level, $z = 0$: $m_h = \frac{1}{\sin h}$,

Linke's turbidity factor (T_L):

Linke's turbidity factor provides an assessment of atmospheric extinction by gas molecules and aerosols. Its average value is given by the following equation:

$$T_L = 2.5 + 16 \cdot \beta_A + 0.5 \cdot \ln w \tag{5}$$

where:

- β_A is the turbidity coefficient or Angström coefficient defined based on the number of aerosols contained in a unit of atmospheric mass vertically at the measurement location. This turbidity coefficient therefore characterizes the clarity of the sky. Thus, $\beta_A = 0.02$ corresponds to a dark blue sky, $\beta_A = 0.05$ to a clear blue sky, $\beta_A = 0.10$ to a pale blue sky, and $\beta_A = 0.20$ to a washed-out or milky blue sky.
- w is the height of condensable water (in cm). It corresponds to the thickness of water that would be obtained by condensing all the water vapor contained in a hypothetical cylinder with a generator parallel to the sun's rays. This height can be determined by radiosondes. It is related to the water vapor pressure e (in mbar) at ground level at ambient temperature by Hann's empirical formula: $w = 0.17 \cdot e$.

The atmospheric parameters used in the calculation of the Linke turbidity factor, notably the Angström coefficient (β_A) and the condensable water height (w), were estimated based on typical climate data for the Kankan region, drawn from the literature and regional meteorological databases.

In the absence of direct local measurements for the period in question, these parameters were assumed to be constant and representative of atmospheric conditions during the dry season, characterized by low relative humidity and moderate aerosol concentrations.

The diffuse radiation received on the inclination plane i (D_i^*)

$$D_i^* = \frac{1+\cos i}{2} \cdot D_0^* + \frac{1-\cos i}{2} \cdot a_1 \cdot G_0^* \tag{6}$$

With:

- a_1 : albedo, which corresponds to the fraction of solar radiation energy received by a surface from the atmosphere that is scattered back toward it.
- G_0^* : global radiation on a horizontal plane.
- D_0^* : diffuse atmospheric radiation on a horizontal plane.

Diffuse atmospheric radiation makes it possible to evaluate the intensity of radiation scattered by the sky towards the ground, taking into account the atmospheric turbidity factor T_L.

$$D_0^* = \frac{\overline{I_0^*}}{25} \cdot (\sin h)^{\frac{1}{2}} \left[T_L - 0.5 - (\sin h)^{\frac{1}{2}} \right] \tag{7}$$

The total radiation on the horizontal plane is given by the following expression:

$$G_0^* = (1270 - 56 \cdot T_L) \cdot (\sin h)^{\frac{T_L+36}{33}} \tag{8}$$

The results of the comparison between the code and the actual data measured on site are given in section 3.1 of the analysis and interpretation of results. This comparison is made for the first day of measurements: April 12, 2025.

2.2.2. Study of the Correlation between the Illuminance Obtained through the Code and the Data Measured on Site

To study the correlation between these two sets of data, namely:

- Data obtained through the code: Y_{code}
- Data measured on site: Y_{site}

We will proceed as follows:

- Plot on the same graph:

The evolution of the two data sets (Y_{code} et Y_{site}), to see how they evolve in relation to each other over time.

- Calculate the correlation coefficient:

Evaluating the correlation coefficient allows us to assess the quality of the relationship between different variables by measuring the strength and intensity of their connection. Given the nature of the data analyzed, the coefficient used is **Pearson**'s, defined by the following expression [23] [24]:

$$r = \frac{\sum_{i=1}^{n}\left(X_i - \bar{X}\right)\left(Y_i - \bar{Y}\right)}{\sqrt{\sum_{i=1}^{n}\left(X_i - \bar{X}\right)^2 \sum_{i=1}^{n}\left(Y_i - \bar{Y}\right)^2}} \tag{9}$$

where:

- ✓ X_i and Y_i are the values at each moment;
- ✓ $\bar{X}$ and $\bar{Y}$ are the averages;
- ✓ r varies between −1 and +1.
- ✓ n : is the number of data points or samples of the variables

The interpretation of the coefficient r is based on the thresholds commonly proposed in the literature [25], presented in **Table 1**. This is followed by verification of the statistical significance of the coefficient using the t-test (**Table 2**), then evaluation using the p-value method [26] [27] (**Table 3**).

Table 1. Correlation coefficient values.

No.	Correlation coefficient value (r)	Interpretation
1	+0.9 à 1	Very strong positive correlation
2	+0.5 à + 0.9	Moderate to strong correlation
3	0 à + 0.5	Weak correlation
4	0	No correlation
5	−0.5 à 0	Weak negative correlation
6	−1 à − 0.9	Very strong negative correlation

The significance test checks whether the correlation observed between the two groups of values is statistically significant. The statistical significance of r is tested using Student's t-statistic [28]:

$$t = \frac{r\sqrt{n-2}}{\sqrt{1-r^2}} \tag{10}$$

where:

- ✓ r : is Pearson's correlation coefficient;
- ✓ n : is the number of points, or data points;
- ✓ $n-2$: is the degree of freedom (for two distinct parameters).

The significance test consists of comparing the calculated value of t with the corresponding critical value (T.5%), obtained from Student's table [29], in order to evaluate the hypothesis under study.

- H_0 represents the null hypothesis, for which $r = 0$: "there is no real correlation between X and Y".
- H_1 represents the alternative hypothesis $r \neq 0$: «there is a real correlation between X and Y, which may be positive or negative, depending on the sign of r ».

The two hypotheses and the interpretation of the significance test results are summarized in Table 2 below:

Table 2. Significance test and its interpretation.

Value of t	Hypothesis	Interpretation	Decision
$t <$ T.5%	H_0, Null hypothesis ($r = 0$)	No significant relationship between X and Y	No evidence of a real correlation
$t \geq$ T.5%	H_1, Alternative hypothesis ($r \neq 0$), H_0 is rejected.	There is a significant relationship between X and Y	The correlation is not due to chance

For the test based on the p-value method, the critical value is also determined from the student's table. The p-value represents the probability of obtaining a statistic at least as extreme as the one observed when the null hypothesis is true. Its interpretation is based on a comparison between the p-value and the significance threshold α, generally set at 0.05, as shown in Table 3 below.

Table 3. Test using the p-value method [26] [27].

p-value		Interpretation	Decision
$p < \alpha$	$p < 0.01$	Highly significant correlation	We reject H_0, H_1 is true.
	$0.01 \leq p < 0.05$	Significant correlation	
$p \geq \alpha$	$0.05 \leq p < 0.10$	Weakly significant correlation	We accept H_0
	$p \geq 0.10$	Non-significant correlation	

3. Analysis and Interpretation of Results

3.1. Results of the Comparison between the Code and Actual Data

The experiment was conducted on the first day of the measurement campaign, April 12, 2025. The data generated by the code were compared with those recorded in situ on the same day.

For the model input parameters, the date corresponding to this date (April 12, 2025) is n = 102. The study site selected is the University of Kankan, whose geographical coordinates are as follows: longitude L = 9.3069˚W, latitude Φ = 10.3835˚N, and altitude z = 0.38 km. The albedo a1 was taken as 0.25, as this corresponds to the fraction of incident energy that is scattered by the gravel on the ground where the solar panel was installed. An inclination of i = 15˚ and a south orientation γ = 0˚ were taken.

In fact, the choice of albedo $a_1 = 0.25$ is justified by the nature of the soil at the experimental site, which consists mainly of gravel and light-colored surfaces with moderate reflectivity.

The tilt $i = 15^\circ$ was selected in accordance with the site's latitude (≈10°N) to optimize annual solar radiation capture, while taking into account practical installation constraints. The south-facing orientation ($\gamma = 0^\circ$) corresponds to the standard configuration for maximizing solar exposure in the Northern Hemisphere.

The results of the measurements were compared with those given by the evaluation code. The curves of the results obtained show that the variation in global daily irradiance is almost in agreement with the evolution of the measured solar irradiance. This comparison is presented in the graph in Figure 13 below.

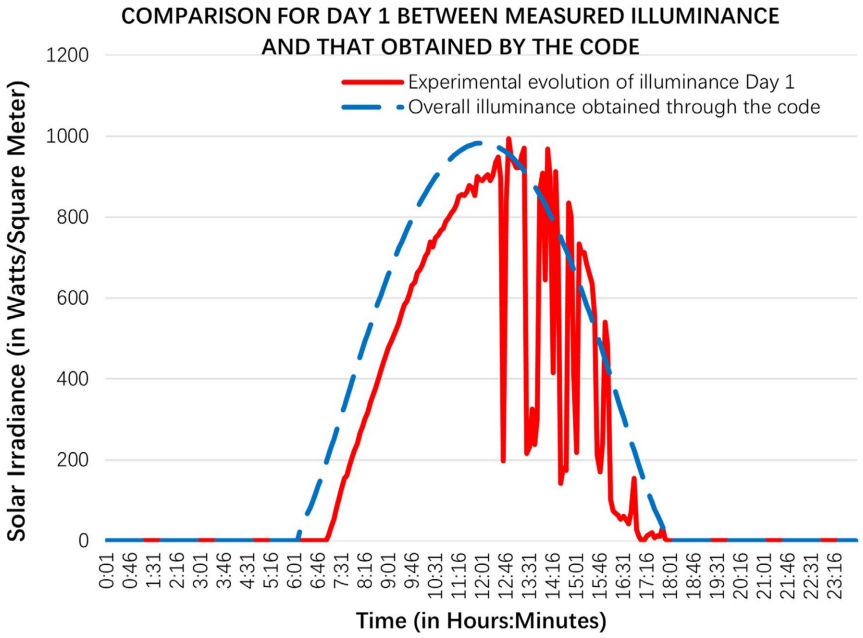

Figure 13. Comparison for day 1 (April 12, 2025) between measured illuminance and that obtained by the code.

3.2. Results of the Study of the Correlation between Experimental Data and Code Data

- **Correlation analysis**

Correlation analysis and significance testing of these two sets of solar irradiance data, namely those obtained from the code and those measured on site, shown in the previous figure (Figure 13), give us the following results:

- Correlation coefficient: $r = 0.9996$
- Coefficient of determination: $R^2 = 0.9992$
- Test statistical value: $t = 118.7$
- Value: $\text{p-value} = 2.23 \times 10^{-268} \approx 0$

Interpretation of the results of r et R^2

The values of r and R^2 found show an almost perfect and positive correlation between the two variables, which indicates the extent to which variations in one of the two groups of variables: Y_{code} or Y_{site} can be predicted by the other.

Interpretation of the *t*-value

The calculation of the test statistic gives a result of: t= 118.7; this value, which is well above the critical threshold of 1.97 for α=5%, shows that the correlation between Y_{code} and Y_{site} is highly significant. We can therefore conclude that there is a very strong positive linear correlation between the two variables.

Interpretation of the p-value result

The p-value found ($2.23\times10^{-268} \approx 0$) is well below 0.01; thus, hypothesis H_0 is rejected, and H_1 is true, which explains a "highly significant correlation." In other words, the variation of the two variables coincides perfectly over time.

- **Equation of the adjustment line**

The analysis of the correlation between the two solar irradiance values was completed by evaluating and constructing the adjustment line shown in Figure 14.

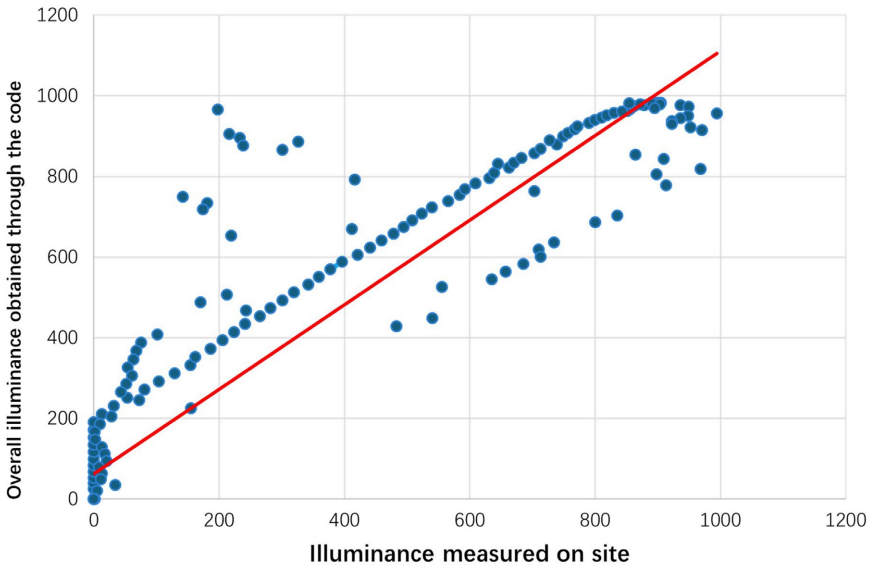

Figure 14. Linear adjustment of the illuminance obtained by the code and that measured on site.

We find that this adjustment line obtained by linear regression closely follows the trend of the data.

Indeed, the scatter plot of the illuminance measured on site as a function of the overall illuminance obtained through the code shows a clear positive linear relationship. The adjustment line obtained by linear regression closely follows the data trend, with a high R^2, thus confirming that the model (developed code) explains most of the variation in illuminance measured on site.

The measurements taken in the Kankan region were made between April 12 and 18, 2025, taking into account strong solar radiation, with a peak solar irradiance of close to 1000 W/m^2 around midday, considered to be the standard ground

irradiance. This observation is consistent with the work of Abdellatif Oudrane on the remarkable intensity of irradiance in the intertropical zone. Thus, despite the immense energy potential, its availability remains subject to fluctuations caused by atmospheric dust, humidity, and the angle of incidence of solar radiation. These factors have an impact on solar energy yield in this region. Therefore, the regularity of this daily solar curve shows the progression of radiation to its maximum height, with variations due to climatic conditions. However, stability and meteorological variation show continuous observation with adaptation of the production and storage system. This measurement shows harmonious management of illumination and demand, improving the efficiency of the system and reducing losses.

It should be noted, however, that the results presented in this study are based on an observation period limited to one week of measurements during the dry season. This relatively short duration does not allow for the full capture of seasonal variability in solar radiation, particularly the significant impact of cloud cover and humidity during the rainy season. Consequently, extending the measurements over a full year would be necessary for a more comprehensive characterization of the local solar resource.

4. Conclusions

The objective of this study was to evaluate solar irradiance in the urban area of Kankan based on experimental measurements taken between April 12 and 18, 2025, and to examine the relevance of a code for estimating solar resources applied under the same conditions. The results obtained highlight a particularly high solar potential, confirming the major energy interest of this area located in Upper Guinea.

The data collected using an autonomous pyranometer revealed a regular and well-structured daily cycle, with maximum values averaging 1000 to 1100 W/m^2 around the zenith. Analysis of the seven daily curves showed a high degree of consistency in the irradiation profile, despite fluctuations linked to atmospheric variability (clouds, dust, and humidity). The average curve obtained for the period studied confirms the overall stability of the solar resource, with a high central plateau between 10:00 a.m. and 2:00 p.m., clearly illustrating the availability of a reliable and abundant solar resource.

The comparison between the experimental data and the values obtained from the solar resource assessment code revealed a very strong linear correlation, as evidenced by a high correlation coefficient, a test statistic well above the critical threshold, and a p-value of less than 0.01. These results demonstrate the validity of the model used and its ability to accurately represent the actual behavior of solar radiation at the site studied. In addition, the adjustment line obtained reinforces the idea that the model is a reliable tool for estimating solar resources in similar contexts.

This study thus contributes significantly to a better characterization of the solar

potential of the city of Kankan, where energy demand remains high and access to electricity is still limited. The results provide a solid scientific basis for the design and optimization of photovoltaic installations, particularly in the context of urban or rural electrification projects. They also pave the way for future work on extending the time frame of measurements, seasonal radiation modeling, solar forecasting, and evaluating the actual performance of photovoltaic systems installed in the region.

This study confirms that Upper Guinea, and particularly the city of Kankan, has remarkable solar resources that could play a key role in the national energy transition and in promoting sustainable development based on renewable energies.

The results obtained, based on validated local experimental data, significantly reduce the uncertainties associated with solar resource estimates. This improvement in the accuracy of input data directly contributes to more reliable and optimized sizing of photovoltaic systems by enabling a more accurate estimate of energy yield.

Consequently, this promotes the installation of photovoltaic systems better suited to local conditions, with controlled investment costs and improved performance.

Conflicts of Interest

The authors declare no conflicts of interest regarding the publication of this paper.

References

[1] Solargis (2025) Solar Resource Maps & GIS Data for 200+ Countries. https://solargis.com/resources/free-maps-and-gis-data?locality=guinea

[2] CrossBoundary Energy (2025) Measuring Solar Irradiation in Africa: A Case for Change. https://crossboundaryenergy.com/measuring-solar-irradiation-africa-report/

[3] Sawadogo, W., Bliefernicht, J., Fersch, B., Salack, S., Guug, S., Ogunjobi, K.O., *et al.* (2023) Global Horizontal Irradiance in West Africa: Evaluation of the WRF-Solar Model in Convection-Permitting Mode with Ground Measurements. *Journal of Applied Meteorology and Climatology*, **62**, 835-851. https://doi.org/10.1175/jamc-d-22-0186.1

[4] Ernst, M., Thomson, A., Haedrich, I. and Blakers, A. (2016) Comparison of Ground-Based and Satellite-Based Irradiance Data for Photovoltaic Yield Estimation. *Energy Procedia*, **92**, 546-553. https://doi.org/10.1016/j.egypro.2016.07.139

[5] Kumar, D.S., Yagli, G.M., Kashyap, M. and Srinivasan, D. (2020) Solar Irradiance Resource and Forecasting: A Comprehensive Review. *IET Renewable Power Generation*, **14**, 1641-1656. https://doi.org/10.1049/iet-rpg.2019.1227

[6] Esposito, E., Leanza, G. and Di Francia, G. (2024) Comparative Analysis of Ground-Based Solar Irradiance Measurements and Copernicus Satellite Observations. *Energies*, **17**, Article 1579. https://doi.org/10.3390/en17071579

[7] Oliveira, M., Silva Lopes, H., Mendonça, P., Tenpierik, M. and Silva, L.T. (2024) Solar Radiation Measurement Tools and Their Impact on in Situ Testing—A Portuguese

Case Study. *Buildings*, **14**, Article 2117. https://doi.org/10.3390/buildings14072117

[8] Li, B., Liu, Z., Wu, Y., Wang, P., Liu, R. and Zhang, L. (2023) Review on Photovoltaic with Battery Energy Storage System for Power Supply to Buildings: Challenges and Opportunities. *Journal of Energy Storage*, **61**, Article 106763. https://doi.org/10.1016/j.est.2023.106763

[9] León Gómez, J.C., De León Aldaco, S.E. and Aguayo Alquicira, J. (2023) A Review of Hybrid Renewable Energy Systems: Architectures, Battery Systems, and Optimization Techniques. *Eng*, **4**, 1446-1467. https://doi.org/10.3390/eng4020084

[10] Martinez Lopez, V.A., Žindžiūtė, U., Ziar, H., Zeman, M. and Isabella, O. (2022) Study on the Effect of Irradiance Variability on the Efficiency of the Perturb-and-Observe Maximum Power Point Tracking Algorithm. *Energies*, **15**, Article 7562. https://doi.org/10.3390/en15207562

[11] Diarra, M. (2022) Consultant en évaluation environnementale et sociale (MS. Env.). https://tinyurl.com/585zm7hp

[12] Diallo, M.S. (2025) Les ONG locales de développement et la question de pérennisation de leurs acquis dans la préfecture de kankan (Guinée). https://www.memoireonline.com/12/13/8235/Les-ONG-locales-de-developpement-et-la-question-de-perennisation-de-leurs-acquis-dans-la-prefectu.html?utm_source=chatgpt.com#google_vignette

[13] Mapcarta (2025) Kankan. https://mapcarta.com/N2746237191

[14] (2025) Carte topographique Région de Kankan. Cartes Topographiques. https://fr-be.topographic-map.com/map-3mw39m/R%C3%A9gion-de-Kankan/

[15] https://documents1.worldbank.org/curated/en/496111468244207994/txt/E19810v10FRENCH0Guinea0P1136080EA0v1.txt?utm_source=chatgpt.com

[16] Banque mondiale (2010) Guinée—Rapport d'évaluation environnementale (P113608). Rapports de la Banque mondiale, 108. https://documents1.worldbank.org/curated/en/496111468244207994/pdf/E19810v10FRENCH0Guinea0P1136080EA0v1.pdf

[17] République de Guinée, Ministère des Travaux Publics (2014) Rapport final EIES des 14 ponts de Kankan. Rapport d'Étude d'Impact Environnemental et Social, 535. https://tinyurl.com/4t8a3fve

[18] Banque mondiale (2018) Guinée—Deuxième opération de politique de réforme budgétaire et de développement de la croissance (FGR2). Rapports de la Banque mondiale, 41. https://fr.scribd.com/document/862447509/Guinea-Fr-Sow-Fgr2

[19] Diallo, A.L. (2025) Participation des populations au développement local: Cas de la commune rurale de Koumban, préfecture de Kankan (Guinée). https://www.memoireonline.com/01/12/5103/Participation-des-populations-au-developpement-local-cas-de-la-commune-rurale-de-Koumban-prefect.html

[20] Scribd (2025) Annuaire INS 2019 Opt. https://www.scribd.com/document/662544963/Annuaire-INS-2019-Opt

[21] Camara, M.A. (2011) Modélisation du stockage de l'énergie photovoltaïque par supercondensateurs. https://theses.fr/2011PEST1071?utm_source=chatgpt.com

[22] Communay, P.H. (2002) Héliothermique: Le gisement solaire, méthodes et calculs. Groupe de Recherche et d'édition.

[23] Montgomery, D.C. and Runger, G.C. (2014) Applied Statistics and Probability for Engineers. John Wiley & Sons Inc.

[24] Devore, J. (2016) Probability and Statistics for Engineering and the Sciences. Cengage

Learning.

[25] Evans, J.D. (1996) Straightforward Statistics for the Behavioral Sciences. Brooks/Cole Pub Co.

[26] Wasserman, L. (2004) All of Statistics: A Concise Course in Statistical Inference. https://thisislinyu.github.io/DLSPH/Comps/books/all_of_statistics.pdf

[27] Agresti, A. and Finlay, B. (2009) Statistical Methods for the Social Sciences. Pearson.

[28] Wackerly, D., Mendenhall, W. and Scheaffer, R. (2008) Mathematical Statistics with Applications. Thomson Brooks/Cole.

[29] Zimmerman, D., Tanis, E. and Hogg, R. (2019) Probability and Statistical Inference. 9th Edition, Pearson.